

Electronic Supplementary Information

Design of melem-based supramolecular assemblies for the synthesis of polymeric carbon nitrides with enhanced photocatalytic

Jiawei Xia^a, Neeta Karjule^a, Biswajit Mondal^a, Jiani Qin^a, Michael Volokh^a, Lidan Xing^b and Menny Shalom^{a,*}

^aDepartment of Chemistry and Ilse Katz Institute for Nanoscale Science and Technology, Ben-Gurion University of the Negev, Beer-Sheva 8410501, Israel.

^bSchool of Chemistry, South China Normal University, Guangzhou 510006, China.

*Corresponding author:

Prof. Menny Shalom, E-mail: mennysh@bgu.ac.il

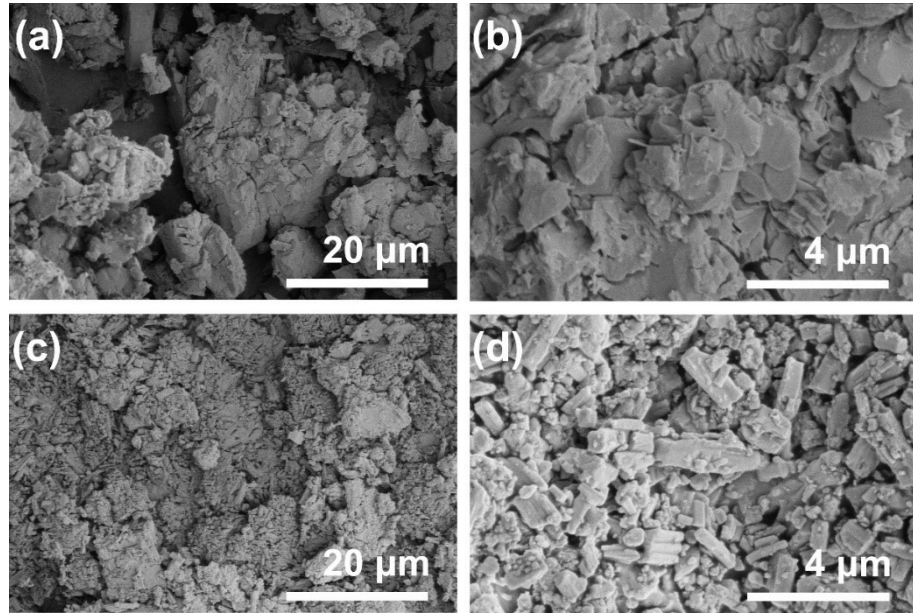


Fig. S1 SEM images of (a, b) melem and (c, d) Me at different magnifications.

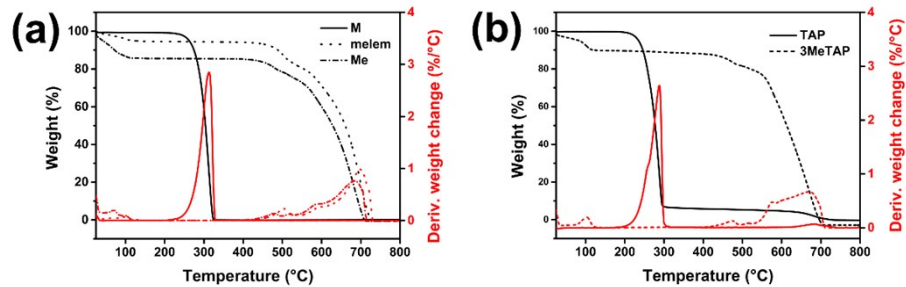


Fig. S2 TGA analysis of (a) M, melem, and Me, (b) TAP and 3MeTAP supramolecular assembly.

Thermal gravimetric analysis (TGA) studies show a considerable weight loss of 90 wt.% detected at ~300 °C for TAP, whereas melem and Me are thermally stable up to ~450 °C (Fig. S2a). In stark contrast to TAP alone, 3MeTAP shows no mass loss at 300 °C and retains its thermal stability up to 450 °C as a result of the interaction between TAP and Me (Fig. S2b). We assign the minor weight losses at around 100 °C in all melem-containing samples to the absorbed or adsorbed water from the ambient environment.

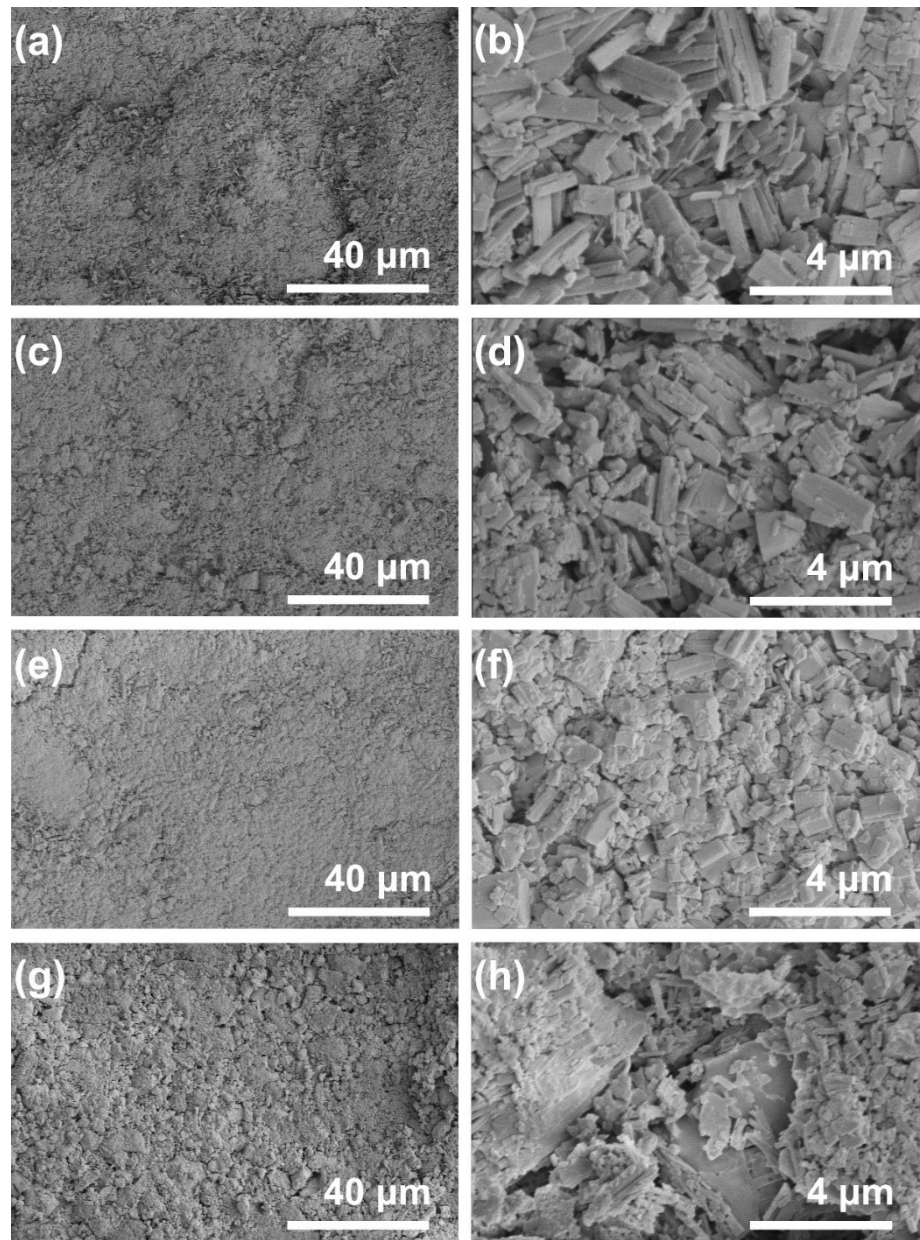


Fig. S3 SEM images of (a, b) 3MeM, (c, d) 3MeCA, (e, f) 3MeCDATA, and (g, h) 3MeTCA at different magnifications.

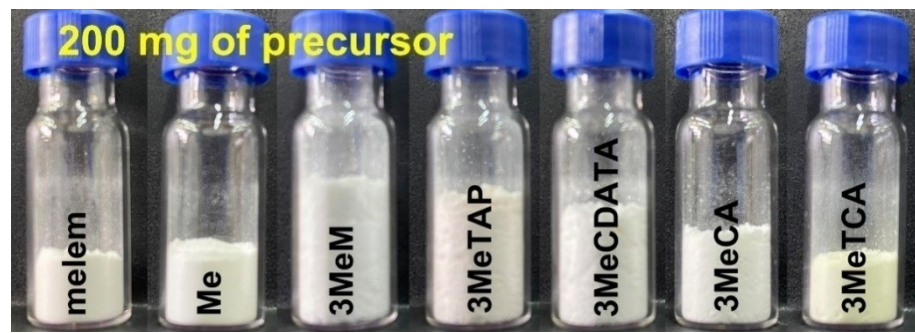


Fig. S4 Digital photos of vials filled with 200 mg of precursor powders.

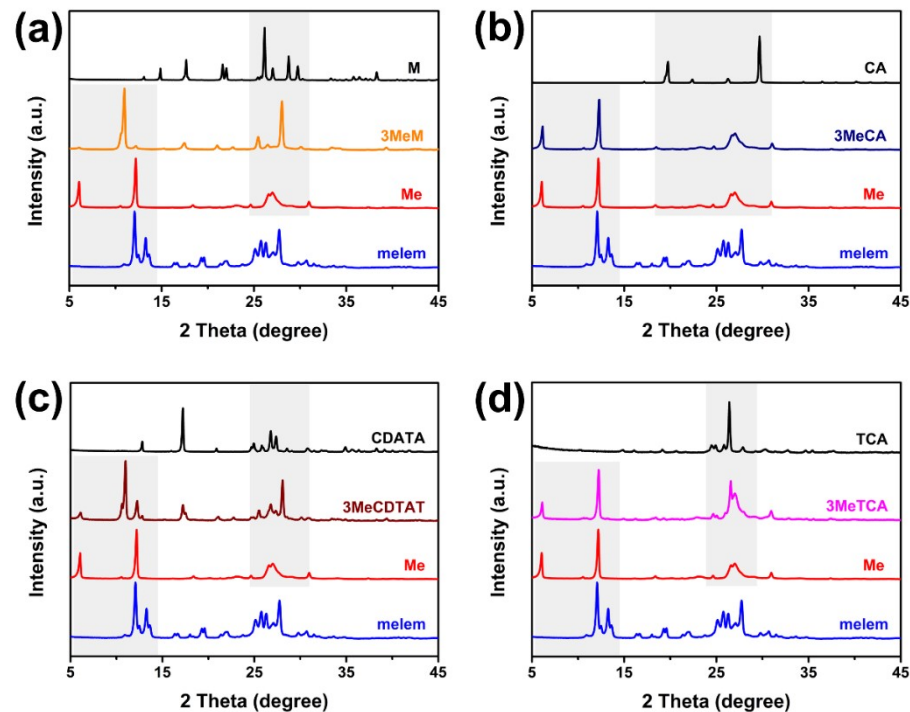


Fig. S5 XRD patterns of melem (blue) and Me (red) compared with (a) M, (b) CA, (c) CDTATA, and (d) TCA as well

as their corresponding binary supramolecular assemblies with melem at a 1:3 molar ratio.

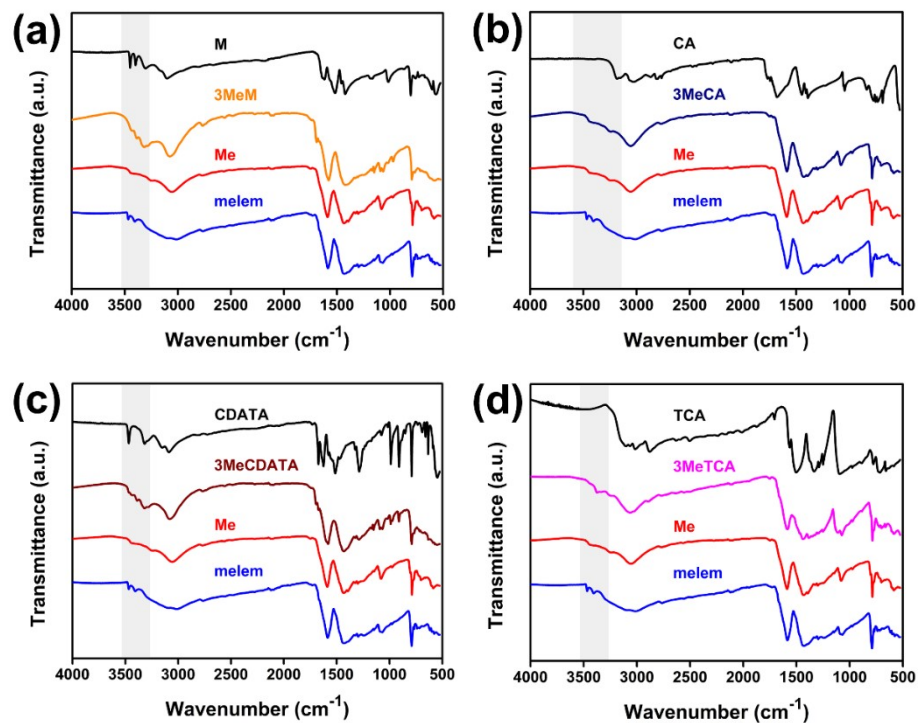


Fig. S6 FTIR spectra of melem (blue) and Me (red) compared with (a) M, (b) CA, (c) CDATA, and (d) TCA as well as their corresponding binary supramolecular assemblies with melem at a 1:3 molar ratio.

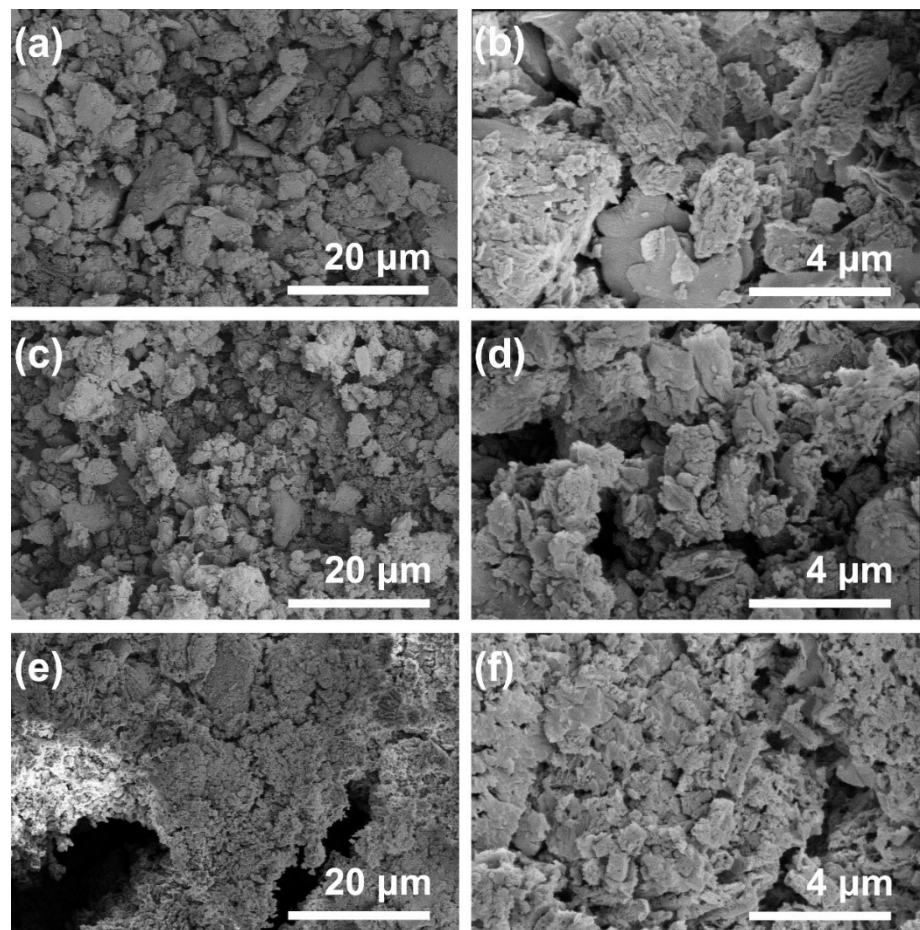


Fig. S7 SEM images of (a, b) CN-M, (c, d) CN-melem, and (e, f) CN-Me at different magnifications.

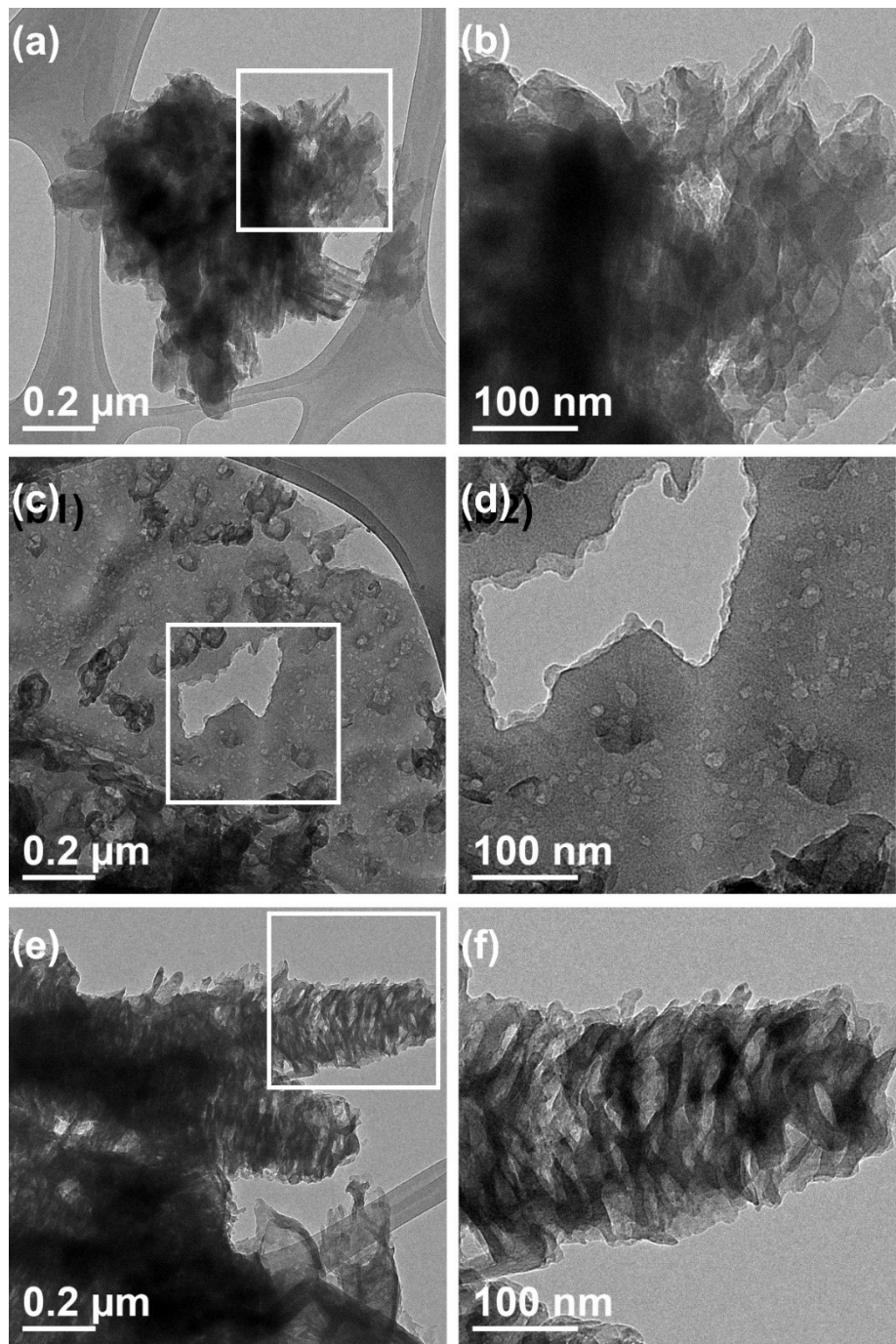


Fig. S8 TEM images of (a, b) CN-M, (c, d) CN-melem, and (e, f) CN-Me at different magnifications. The white square frame on the left indicates the magnified area shown in the corresponding image on the right.

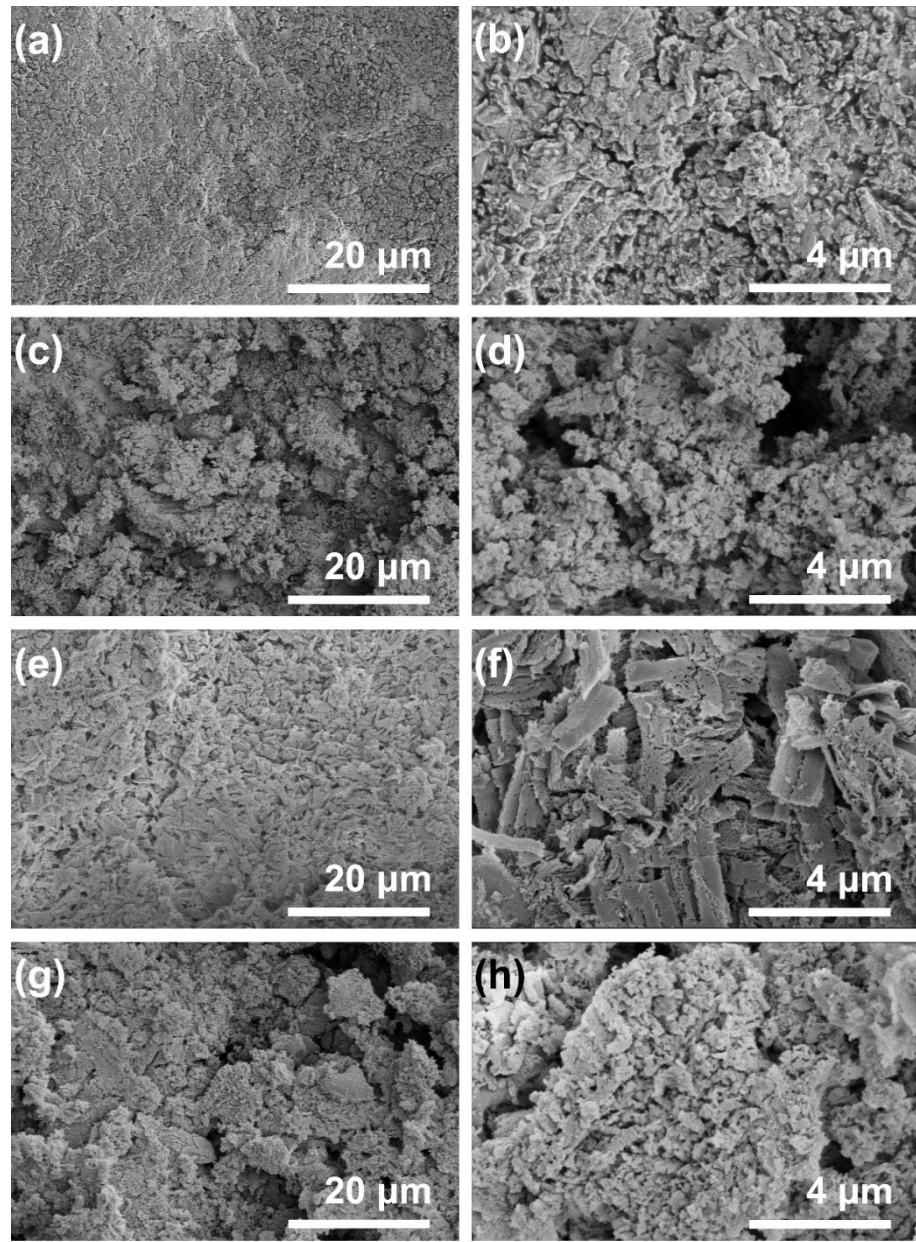


Fig. S9 SEM images of (a, b) CN-3MeM, (c, d) CN-3MeCA, (e, f) CN-3MeCDATA, and (g, h) CN-3MeTCA at different magnifications.

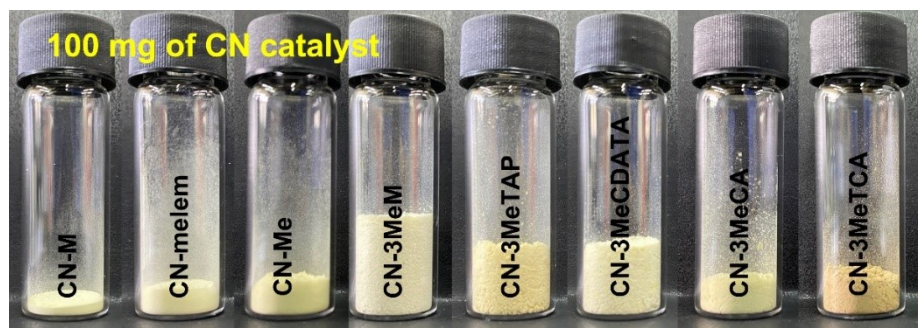


Fig. S10 Digital photos of vials filled with 100 mg of CN materials (prepared from the precursor powders shown in Fig. S4).

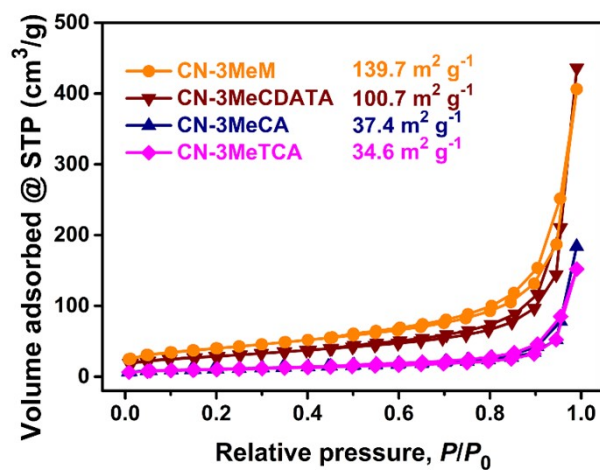


Fig. S11 Nitrogen adsorption-desorption isotherms of CN-3MeM, CN-3MeCDATA, CN-3MeCA, and CN-3MeTCA. The values in the legend are the specific surface area calculated using the BET model.

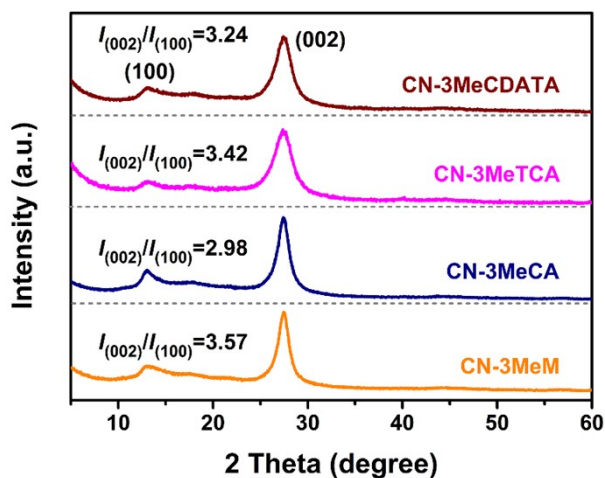


Fig. S12 XRD patterns of CN-3MeM, CN-3MeCA, CN-3MeCDATA, and CN-3MeTCA.

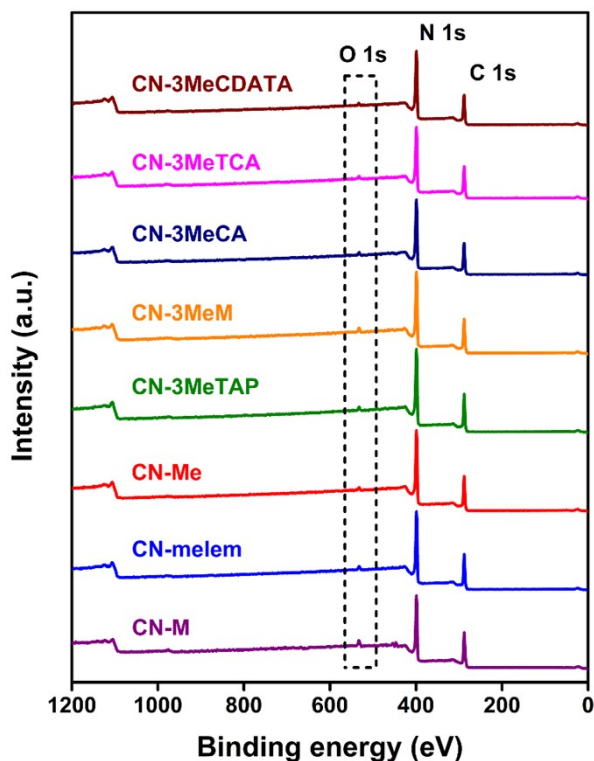


Fig. S13 Global XPS spectra of CN materials.

A global X-ray photoelectron spectroscopy (XPS) analysis of the CN materials (Fig. S13) reveals C and N as the main elements in the photocatalysts; the small portion of O species probably originates from the surrounding environment during the thermal condensation process.

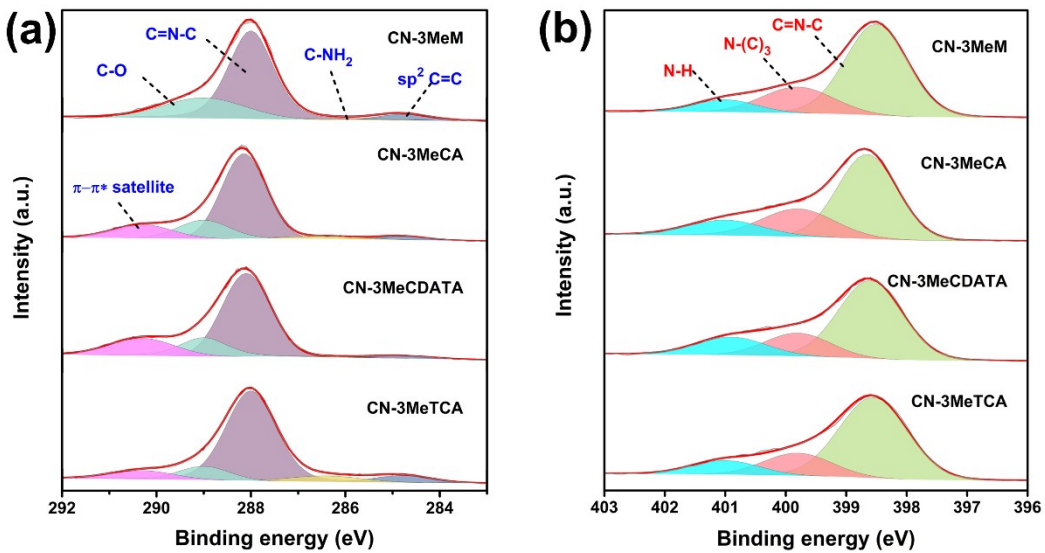


Fig. S14 (a) C 1s and (b) N 1s high-resolution XPS spectra of CN-3MeM, CN-3MeCA, CN-3MeCDATA, and CN-3MeTCA materials.

The C 1s spectra of CN-3MeCA, CN-3MeCDATA, and CN-3MeTCA materials exhibit similar fitted peaks to those of CN-M, CN-melem, CN-Me, CN-3MeM, and CN-3MeTAP, but with one additional small peak centered at 290.3 eV, corresponding to the $\pi-\pi^*$ transition loss.¹ All the investigated CN materials show similar high-resolution XPS spectra of N 1s, suggesting the existence of N species in the forms of C=N–C, N–(C)₃, and C–NH.^{2,3}

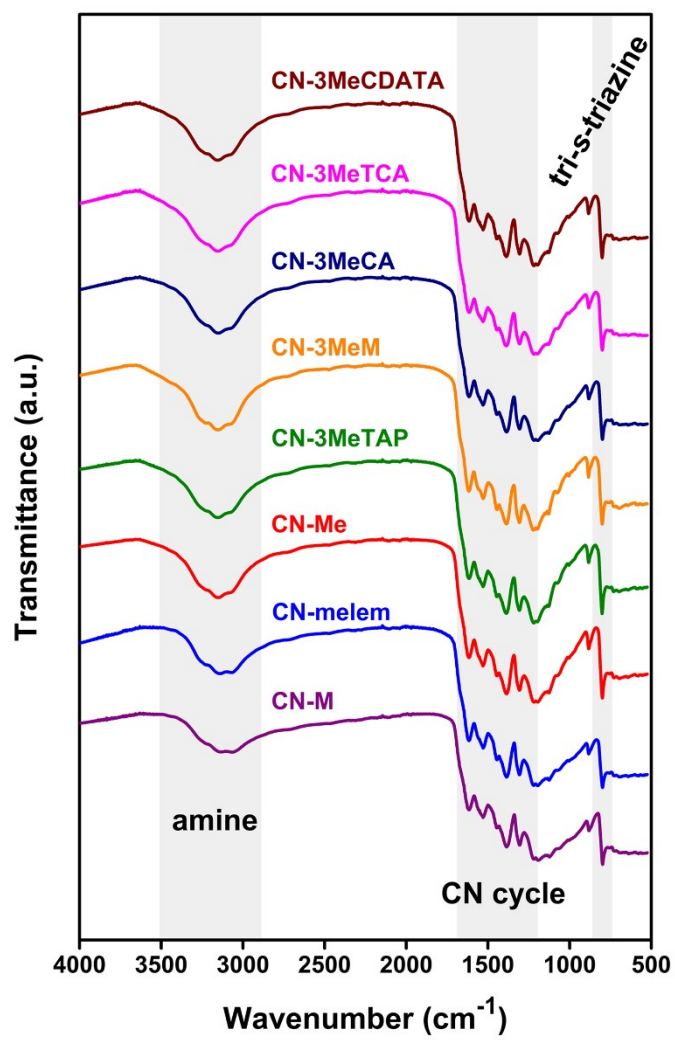


Fig. S15 Survey FTIR spectra of the CN materials. The FTIR spectra were offset for clarity.

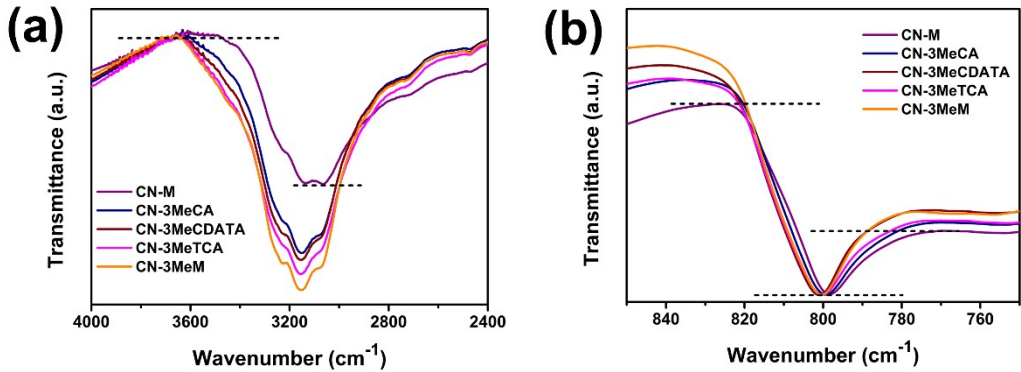


Fig. S16 FTIR spectra of the CN materials at different regions: (a) 2400–4000 cm⁻¹, (b) 750–850 cm⁻¹; the black dashed horizontal lines are a guide to the eye showing the transmittance of CN-M at different positions.

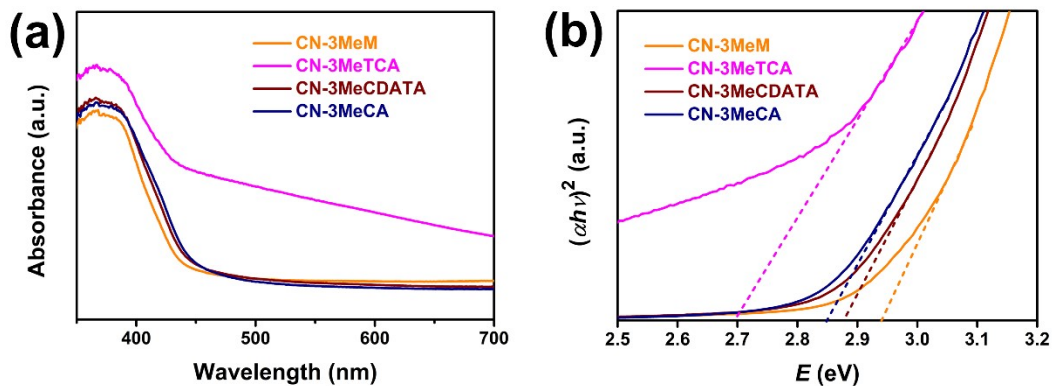


Fig. S17 (a) Absorbance spectra and (b) the corresponding Tauc plot analysis of CN-3MeM, CN-3MeCA, CN-3MeCDATA, and CN-3MeTCA (assuming a direct-band gap).

Compared with CN-M ($E_g = 2.79$ eV), the optical absorption of CN-3MeCA, CN-3MeCDATA, and CN-3MeM is blue-shifted, with E_g s in the 2.85–2.94 eV range. For CN-3MeTCA, a red shift is observed ($E_g = 2.69$ eV). The other CN materials do not reveal significant variations in light absorption and the calculated E_g values are about 2.8 eV (Fig. 4c and Fig. S17b).

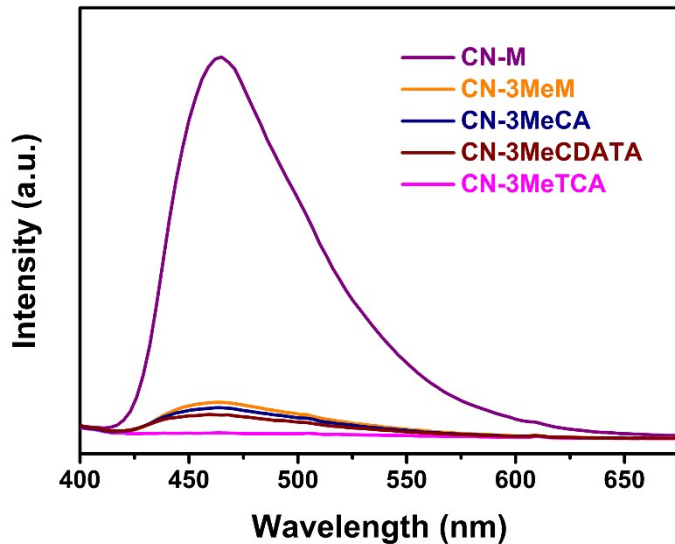


Fig. S18 PL emission spectra of different CN materials. All samples were excited at 370 nm.

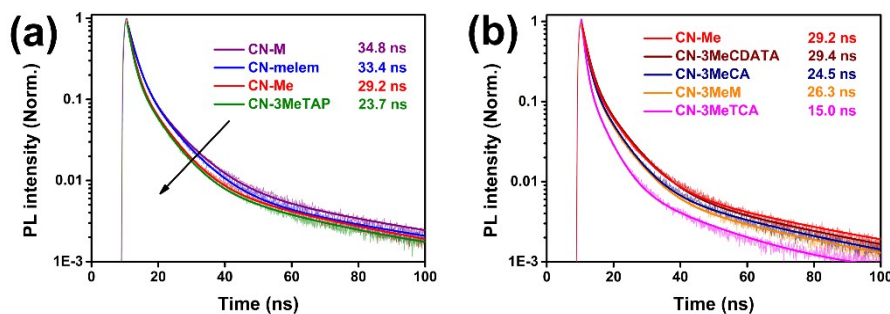


Fig. S19 Time-resolved PL decay spectra of different CN materials (All samples were excited at 370 nm).

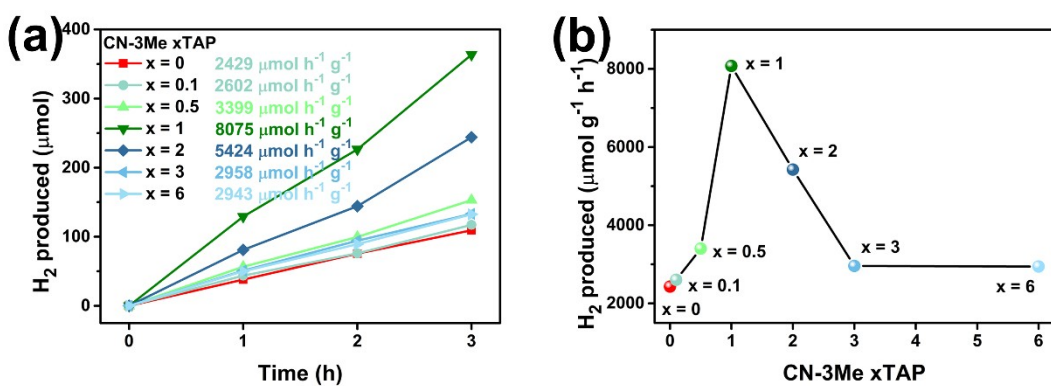


Fig. S20 (a) Time course of H₂ evolution for CN materials synthesized from supramolecular assemblies of melem with different content of TAP; (b) relationship between H₂ evolution rate and TAP content. The experimental data points are connected using lines as a guide to the eye.

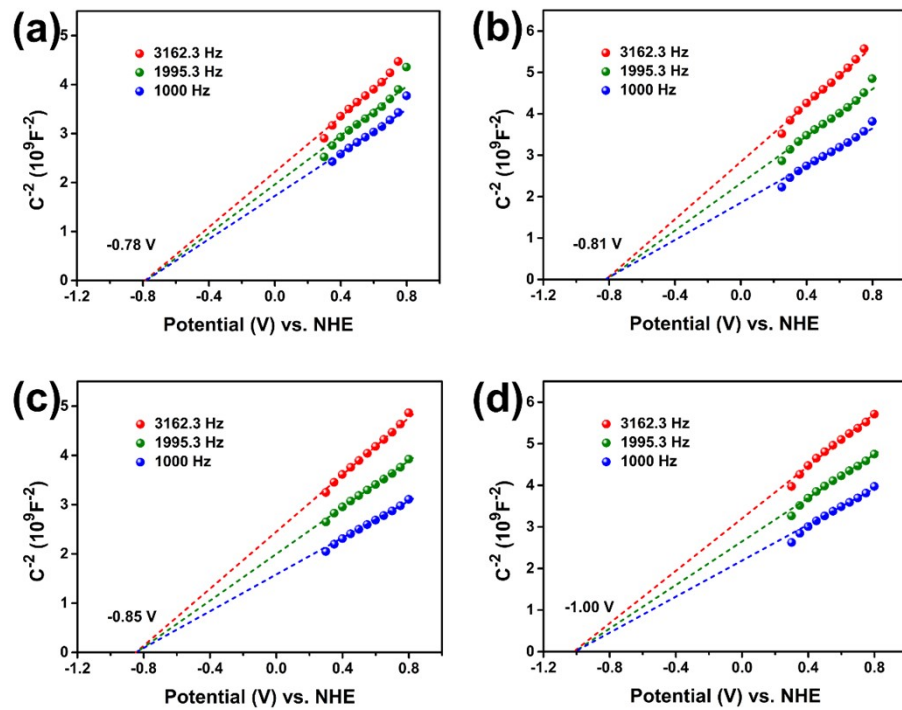


Fig. S21 Mott-Schottky plots of (a) CN-M, (b) CN-melem, (c) CN-Me, and (d) CN-3MeTAP.

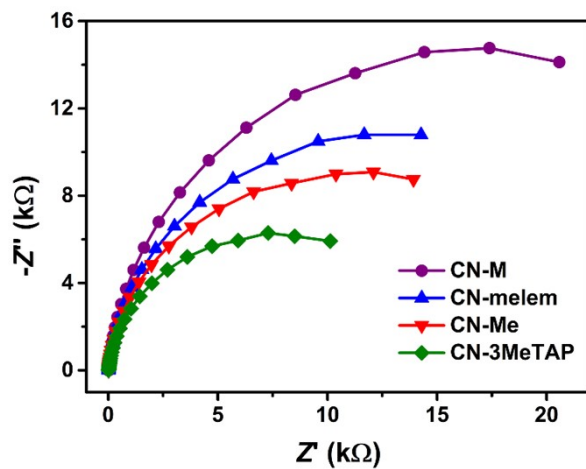


Fig. S22 Nyquist plots (at -0.1 V vs. Ag/AgCl) of different CN materials in 0.1 M Na₂SO₄ aqueous solution.

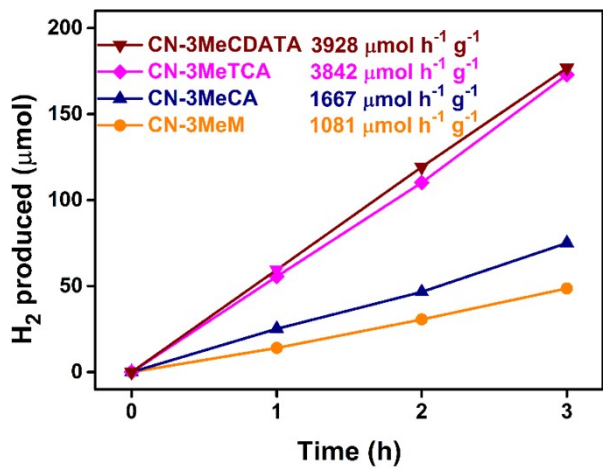


Fig. S23 Time course of H_2 evolution for CN materials under white LED irradiation.

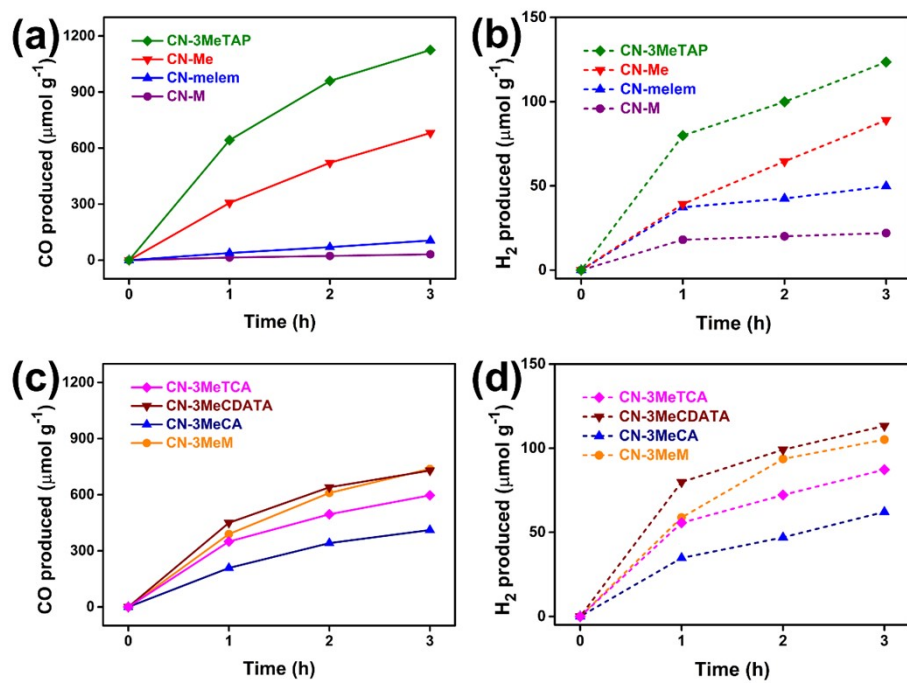


Fig. S24 (a, c) Time course of CO production and (b, d) H_2 evolution for the different CN materials under a white LED irradiation within 3 hours.

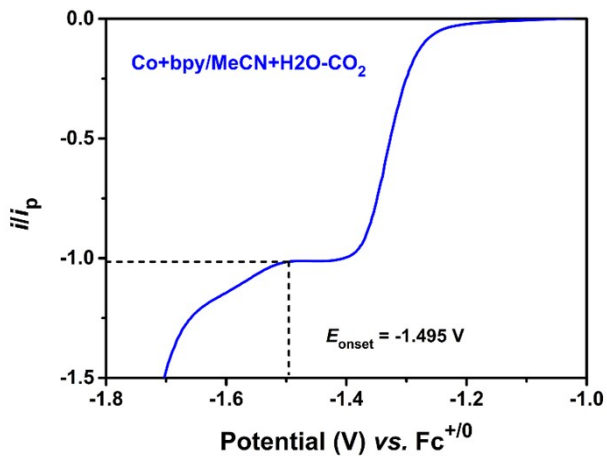


Fig. S25 Normalized LSV curve in the mixed MeCN and H₂O (v/v 4:1) solution containing CoCl₂ (2 mM), bpy (200 mM), and TBACl (100 mM) after CO₂ purging. The LSV curve was normalized by dividing the current value i by that of the peak current (i_p) at -1.44 V (vs. Fc^{+/-}).

Here, we consider the position of the potential at the i/i_p value of 1.015 (> 1 , indicates catalytic turnover) as the onset potential for CO₂RR. The E_{onset} value is -1.495 V vs. Fc^{+/-} and is calculated to be -0.775 V vs. NHE according to the following equation:

$$E_{\text{vs. NHE}} = E_{\text{vs. Fc}^{+/-}} + 0.72.$$

The calibration was conducted in a mixed MeCN and H₂O (v/v 4:1) solution containing TBACl (100 mM) after H₂ purging for 1 h with Pt plate, Pt plate, and Ag/AgCl as the working, counter, and reference electrodes, respectively.

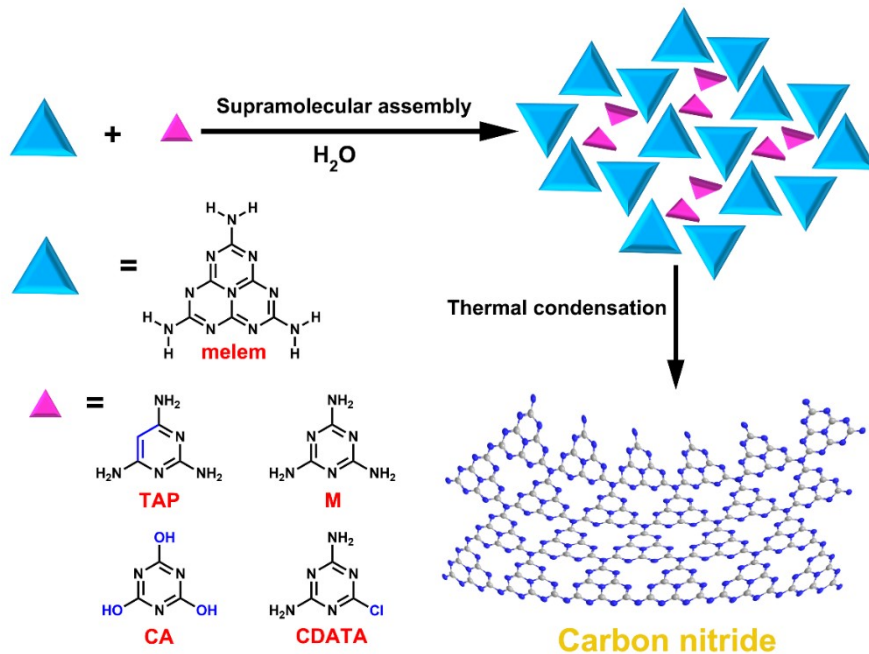


Fig. S26 Schematic illustration of the supramolecular assembly between melem and triazine- or pyrimidine-based small molecules with a 3:1 molar ratio, forming melon-type heptazine-based polymeric carbon nitride.

Table S1 Elemental quantification (at.%) of C, N, and O species in CN materials.

Catalyst	C (at.%)	N (at.%)	O (at.%)	C/N ratio
CN-M	45.41	52.08	2.51	0.872
CN-melem	44.93	53.02	2.05	0.847
CN-Me	44.10	54.25	1.66	0.813
CN-3MeTAP	44.38	53.80	1.82	0.825

Table S2 Comparison of the properties of CN materials as HER photocatalysts

Catalyst	Method	Light source	Catalyst mass	Experimental conditions	H ₂ evolution rate ($\mu\text{mol g}^{-1}\text{h}^{-1}$)	AQY (%)	Ref.
CN from melem-TAP supramolecular assembly	Supramolecular assembly followed by condensation	100 W white LED ($\lambda > 410 \text{ nm}$)	15 mg	3 wt.% Pt, 10% v/v TEOA	8075	15.2 ($\lambda = 405 \text{ nm}$) 3.8 ($\lambda = 430 \text{ nm}$) 2.2 ($\lambda = 550 \text{ nm}$)	This work
High crystalline g-C ₃ N ₄	Two-step thermal condensation from melamine powder	300 W Xe lamp ($\lambda > 420 \text{ nm}$)	50 mg	3 wt.% Pt, 10% v/v TEOA	1031.3	3.8 ($\lambda = 420 \text{ nm}$)	4
Macroscopic foam-like holey ultrathin g-C ₃ N ₄ nanosheets	Three-step thermal condensation from melamine powder	300 W Xe lamp ($\lambda > 400 \text{ nm}$)	20 mg	3 wt.% Pt, 10% v/v TEOA	1144	4.03 ($\lambda = 420 \pm 15 \text{ nm}$)	5
honeycomb-like structured g-C ₃ N ₄	Salt-template-assisted construction	300 W Xe lamp ($\lambda > 400 \text{ nm}$)	50 mg	3 wt.% Pt, 25% v/v lactic acid aqueous solution	459	2.2 ($\lambda = 420 \text{ nm}$)	6
Defect-engineered graphitic carbon nitride nanotubes	Supramolecular assembly followed by thermal condensation	300 W Xe lamp ($\lambda > 400 \text{ nm}$)	10 mg	3 wt.% Pt, 10% v/v TEOA	11850	6.8 ($\lambda = 420 \text{ nm}$)	7
CN from melamine-halogen complexes	Supramolecular assembly followed by thermal condensation	50 W white LED ($\lambda > 410 \text{ nm}$)	15 mg	3 wt.% Pt, 10% v/v TEOA	1815	3.2 ($\lambda = 405 \text{ nm}$)	8
Single-site Rh-phosphide modified carbon nitride	Supramolecular assembly via hydrothermal reaction followed by Rh doping and phosphorization at high temperature	300 W Xe lamp ($\lambda > 400 \text{ nm}$)	20 mg	1 wt.% Pt, 10% v/v TEOA	2078.5	—	9
Soluble g-C ₃ N ₄ nanosheets	Thermal condensation of melamine powder followed by hydrothermal treatment	Four 3 W and 420 nm low-power LEDs	50 mg	1 wt.% Pt, 10% v/v lactic acid solution	359.6	—	10

3D hierarchical porous carbon/graphitic carbon nitride composites	Templating followed by thermal condensation of urea	300 W Xe lamp ($\lambda > 420$ nm)	50 mg	1.5 wt.% Pt, 10% v/v TEOA	1610.7	15 ($\lambda = 420 \pm 10$ nm) 8.9 ($\lambda = 450 \pm 10$ nm) 1.3 ($\lambda = 500 \pm 10$ nm)	11
Simultaneously (S, P, O)-codoped and exfoliated ultrathin g-C ₃ N ₄ nanosheets	Thermal condensation of melamine with S- or P-containing reagents	300 W Xe lamp ($\lambda > 420$ nm)	10 mg	3 wt.% Pt, 20% v/v TEOA	2443	—	12
Graphitic carbon nitride incorporated with <i>p</i> -phenylene	Thermal condensation of melamine followed by a post-polymerization with <i>p</i> -phenylenediamine	300 W Xe lamp ($\lambda > 420$ nm)	100 mg	1 wt.% Pt, 10% v/v TEOA	386	1.64 ($\lambda = 420$ nm)	13
P and C co-doped graphitic carbon nitride	Thermal condensation of melamine and phytic acid mixture	300 W Xe lamp	50 mg	1 wt.% Pt, 20% v/v TEOA	1493.3	2.14 ($\lambda = 420$ nm)	14
Ozone-treated graphitic carbon nitride	Thermal condensation of melamine followed by a post-treatment of ozone	300 W Xe lamp ($\lambda > 420$ nm)	100 mg	0.5 wt.% Pt, 10% v/v TEOA	285	—	15
Se-modified polymeric carbon nitride nanosheets	Thermal condensation of urea followed by a post-polymerization with diphenyl diselenide	300 W Xe lamp ($\lambda > 420$ nm)	50 mg	3 wt.% Pt, TEOA/H ₂ O (10 mL/100 mL)	2600	8.1 ($\lambda = 420$ nm)	16
Crystalline carbon nitride	Two-step polymerization of melamine followed by a post-calcination with NaBH ₄	300 W Xe lamp	50 mg	3 wt.% Pt, 10% v/v TEOA	1280	~6.0 ($\lambda = 405$ nm)	17

Table S3 Comparison of CN materials' properties as CO₂ reduction photocatalysts

Catalyst	Light source	Catalyst mass	Experimental conditions	CO ₂ produced (μmol g ⁻¹)	Ref.
CN from melem-TAP supramolecular assembly	100 W white LED ($\lambda > 410$ nm)	30 mg	MeCN & H ₂ O, 30 °C, CoCl ₂ , 2,2'-bipyridine, TEOA	642 ($t = 1$ h) 959 ($t = 2$ h) 1125 ($t = 3$ h)	This work
Defective graphitic carbon nitride	300 W Xe lamp ($\lambda > 400$ nm)	5 mg	MeCN & H ₂ O, 25 °C, CoCl ₂ , bipyridine, TEOA	284.7 ($t = 5$ h)	18
Cobalt molecular catalyst covalently linked to mesoporous carbon nitride	100 W Xe lamp ($\lambda > 400$ nm)	6 mg	MeCN, 25 °C, PhOH, 1,3-dimethyl-2-phenyl-2,3-dihydro-1H-benzo[d]-imidazole	~125 ($t = 24$ h)	19
Trimesic acid-modified polymeric carbon nitride	300 W Xe lamp	30 mg	MeCN & H ₂ O, 30 °C, CoCl ₂ , 2,2'-bipyridine, TEOA	1433 ($t = 2$ h)	20
Fluorine-modified boron carbon nitride	300 W Xe lamp ($\lambda > 420$ nm)	50 mg	MeCN & H ₂ O, 25 °C, CoCl ₂ , 2,2'-bipyridine, TEOA	310 ($t = 5$ h)	21
Haloid acid induced carbon nitride	300 W Xe lamp ($\lambda > 420$ nm)	30 mg	MeCN & H ₂ O, 30 °C, TEOA	~4 ($t = 1$ h) ~6 ($t = 2$ h) ~7.5 ($t = 3$ h)	22
Porous nitrogen-rich g-C ₃ N ₄ nanotubes	300 W Xe lamp	10 mg	MeCN & H ₂ O, 10 °C, CoCl ₂ , 2,2'-bipyridine, TEOA	338.5 ($t = 3$ h)	23
Polymeric carbon nitride with molecular junctions	300 W Xe lamp ($\lambda > 420$ nm)	50 mg	MeCN & H ₂ O, 30 °C, CoCl ₂ , 2,2'-bipyridine, TEOA	2080 ($t = 13$ h)	24
Zero-dimensional-g-CNQD-coordinated two-dimensional porphyrin MOF hybrids	300 W Xe lamp ($\lambda > 420$ nm)	30 mg	MeCN & H ₂ O, TEOA	~70 ($t = 2$ h)	8
0D/2D heterostructure of QDs TiO ₂ confined in g-C ₃ N ₄ nanosheets	300 W Xe lamp ($\lambda > 400$ nm)	5 mg	MeCN & H ₂ O, 25 °C, CoCl ₂ , bipyridine, TEOA	388.9 ($t = 5$ h)	25
Oxidative polyoxometalates-modified graphitic carbon nitride	300 W Xe lamp ($\lambda > 420$ nm)	50 mg	MeCN & H ₂ O, 20 °C, CoCl ₂ , bipyridine, TEOA	~210 ($t = 2$ h) 896 ($t = 10$ h)	26

Table S4 Selectivity of CO catalyzed by different CN materials

CN material	Selectivity (%)	CN material	Selectivity (%)
CN-M	58.7	CN-3MeM	87.5
CN-melem	67.3	CN-3MeCA	86.9
CN-Me	88.4	CN-3MeTCA	87.2
CN-3MeTAP	90.1	CN-3MeCDATA	86.6

Electronic Supplementary Information References

- 1 J. Xia, Y. Fu, G. He, X. Sun, X. Wang, *Appl. Catal., B*, 2017, **200**, 39.
- 2 C. Zheng, X. Qiu, J. Han, Y. Wu, S. Liu, *ACS Appl. Mater. Interfaces*, 2019, **11**, 42243.
- 3 Y. Zhao, J. Liu, C. Wang, X. Zhang, C. Chen, X. Zhao, J. Li, H. Jin, *J. Power Sources*, 2019, **424**, 176.
- 4 L. Wang, Y. Hong, E. Liu, Z. Wang, J. Chen, S. Yang, J. Wang, X. Lin, J. Shi, *Int. J. Hydrogen Energy*, 2020, **45**, 6425.
- 5 Y. Li, R. Jin, Y. Xing, J. Li, S. Song, X. Liu, M. Li, R. Jin, *Adv. Energy Mater.*, 2016, **6**, 1601273.
- 6 F. Yang, D. Liu, Y. Li, L. Cheng, J. Ye, *Appl. Catal., B*, 2019, **240**, 64.
- 7 Z. Mo, H. Xu, Z. Chen, X. She, Y. Song, J. Wu, P. Yan, L. Xu, Y. Lei, S. Yuan, H. Li, *Appl. Catal., B*, 2018, **225**, 154.
- 8 J. Barrio, A. Grafmüller, J. Tzadikov, M. Shalom, *Appl. Catal., B*, 2018, **237**, 681.
- 9 Z. Chen, Y. Bu, L. Wang, X. Wang, J.-P. Ao, *Appl. Catal., B*, 2020, **274**, 119117.
- 10 X. Wu, X. Wang, F. Wang, H. Yu, *Appl. Catal., B*, 2019, **247**, 70.
- 11 C. Wang, G. Liu, K. Song, X. Wang, H. Wang, N. Zhao, F. He, *ChemCatChem*, 2019, **11**, 6364.
- 12 Q. Liu, J. Shen, X. Yu, X. Yang, W. Liu, J. Yang, H. Tang, H. Xu, H. Li, Y. Li, J. Xu, *Appl. Catal., B*, 2019, **248**, 84.
- 13 H. Gao, Y. Guo, Z. Yu, M. Zhao, Y. Hou, Z. Zhu, S. Yan, Q. Liu, Z. Zou, *ChemSusChem*, 2019, **12**, 4285.
- 14 H. Wang, B. Wang, Y. Bian, L. Dai, *ACS Appl. Mater. Interfaces*, 2017, **9**, 21730.
- 15 X. Liu, H. Ji, J. Wang, J. Xiao, H. Yuan, D. Xiao, *J. Colloid Interface Sci.*, 2017, **505**, 919.
- 16 H. Ou, C. Tang, Y. Zhang, A. M. Asiri, M.-M. Titirici, X. Wang, *J. Catal.*, 2019, **375**, 104.
- 17 W. Ren, J. Cheng, H. Ou, C. Huang, M. M. Titirici, X. Wang, *ChemSusChem*, 2019, **12**, 3257.
- 18 H. Shi, S. Long, J. Hou, L. Ye, Y. Sun, W. Ni, C. Song, K. Li, G. G. Gurzadyan, X. Guo, *Chem. Eur. J.*, 2019, **25**, 5028.
- 19 B. Ma, G. Chen, C. Fave, L. Chen, R. Kuriki, K. Maeda, O. Ishitani, T. C. Lau, J. Bonin, M. Robert, *J. Am. Chem. Soc.*, 2020, **142**, 6188.
- 20 A. Hayat, J. Khan, M. U. Rahman, S. B. Mane, W. U. Khan, M. Sohail, N. U. Rahman, N. Shaista, Z. Chi, M. Wu, *J. Colloid Interface Sci.*, 2019, **548**, 197.
- 21 F. Xing, Q. Liu, M. Song, C. Huang, *ChemCatChem*, 2018, **10**, 5270.
- 22 S. Wan, M. Ou, Q. Zhong, W. Cai, *Carbon*, 2018, **138**, 465.
- 23 Z. Mo, X. Zhu, Z. Jiang, Y. Song, D. Liu, H. Li, X. Yang, Y. She, Y. Lei, S. Yuan, H. Li, L. Song, Q. Yan, H. Xu, *Appl. Catal., B*, 2019, 256.
- 24 Z. Pan, P. Niu, M. Liu, G. Zhang, Z. Zhu, X. Wang, *ChemSusChem*, 2020, **13**, 888.

- 25 H. Shi, S. Long, S. Hu, J. Hou, W. Ni, C. Song, K. Li, G. G. Gurzadyan, X. Guo, *Appl. Catal., B*, 2019, **245**, 760.
- 26 J. Zhou, W. Chen, C. Sun, L. Han, C. Qin, M. Chen, X. Wang, E. Wang, Z. Su, *ACS Appl. Mater. Interfaces*, 2017, **9**, 11689.